GEOPHYSICS, VOL. 72, NO. 5 (SEPTEMBER-OCTOBER 2007); P. A69–A73, 4 FIGS.
10.1190/1.2761967

Interferometric surface-wave isolation and removal

David F. Halliday[1], Andrew Curtis[2], Johan O. A. Robertsson[3], and Dirk-Jan van Manen[3]

ABSTRACT

The removal of surface waves (ground roll) from land seismic data is critical in seismic processing because these waves tend to mask informative body-wave arrivals. Removal becomes difficult when surface waves are scattered, and data quality is often impaired. We apply a method of seismic interferometry, using both sources and receivers at the surface, to estimate the surface-wave component of the Green's function between any two points. These estimates are subtracted adaptively from seismic survey data, providing a new method of ground-roll removal that is not limited to nonscattering regions.

INTRODUCTION

In reflection seismology, surface waves constitute a strong source of noise that is difficult to remove and often obscures the reflected waves in which we are interested. In heterogeneous media, removal of these surface waves by conventional methods (such as *f-k* filtering) is often difficult because their energy is distributed over a wide portion of the *f-k* spectrum. We present a new method of surface-wave removal that can be applied in either the time or frequency domain and has the potential to be effective in media with both homogeneous and heterogeneous near-surface conditions.

We can show that the Green's function accounting for wave propagation between two points in lossless media can be synthesized by crosscorrelations of wavefield recordings made at each point. These wavefields are excited by distributed active or passive (noise) sources. Details of the method differ, depending on the source type (Wapenaar, 2004; van Manen et al., 2005, 2006; Wapenaar and Fokkema, 2006). Such methods have found several applications in seismology, where they are referred to collectively as seismic interferometry.

When using active sources, theory indicates that sources are required to form a surface that bounds the portion of the earth in which we are interested. In practice, this requirement can be relaxed. In the virtual source method of Bakulin and Calvert (2004, 2006), for example, sources are located only at (or near) the earth's surface and receivers are placed in a borehole. Recordings from these sources are used to create virtual sources at the downhole receivers.

In the related field of passive seismic interferometry, crosscorrelations of ambient noise at periods of 5–20 s can produce estimates of the (direct) Rayleigh wave between surface receivers (Shapiro and Campillo, 2004; Shapiro et al., 2005). The authors argue that the Rayleigh-wave component is isolated in these crosscorrelations because (a) Rayleigh waves dominate the Green's function between surface locations, and (b) near-surface noise sources in this relatively low-frequency band preferentially excite Rayleigh waves.

We use a method similar to the virtual source approach but with a very different geometry, where both sources and receivers are located at the surface. Using the same reasoning as Shapiro et al. (2005), we expect (and observe) that our active source method produces interreceiver signals that are dominated by surface waves. In a conventional land seismic survey, the response to surface sources can be recorded explicitly at any planned source and receiver locations. This allows the interferometric interreceiver surface waves to be removed from source-receiver survey data, providing a new method of ground-roll removal (Curtis et al., 2006; Dong et al., 2006). Because interferometry works in any degree of heterogeneity and is shown to work better in more strongly scattering media (Larose et al., 2005), so should this new method.

GUIDED-WAVE CONSTRUCTION IN A TWO-LAYER ACOUSTIC MODEL

Wapenaar and Fokkema (2006) use reciprocity theorems of the correlation type to show that the acoustic Green's function $\hat{G}(\mathbf{x}_B, \mathbf{x}_A, \omega)$ between two points $\mathbf{x}_B$ and $\mathbf{x}_A$ can be determined by

Manuscript received by the Editor January 31, 2007; revised manuscript received May 24, 2007; published online August 21, 2007.
[1]University of Edinburgh, Grant Institute of Earth Science, Edinburgh, Scotland, United Kingdom. E-mail: d.f.halliday@sms.ed.ac.uk.
[2]University of Edinburgh, Grant Institute of Earth Science, Edinburgh, Scotland, United Kingdom, and Edinburgh Collaborative of Subsurface Science and Engineering (ECOSSE). E-mail: andrew.curtis@ed.ac.uk.
[3]WesternGeco London Technology Centre, Schlumberger House, Gatwick, United Kingdom. E-mail: jrobertsson@gatwick.westerngeco.slb.com; dmanen@gatwick.westerngeco.slb.com.

$$\hat{G}^*(\mathbf{x}_B,\mathbf{x}_A,\omega) + \hat{G}(\mathbf{x}_B,\mathbf{x}_A,\omega) = \oint_{\partial D_1} \frac{-1}{j\omega\rho(\mathbf{x})}(\hat{G}^*(\mathbf{x}_A,\mathbf{x},\omega)\partial_i\hat{G}(\mathbf{x}_B,\mathbf{x},\omega) - (\partial_i\hat{G}^*(\mathbf{x}_A,\mathbf{x},\omega))\hat{G}(\mathbf{x}_B,\mathbf{x},\omega))n_i d^2\mathbf{x}, \quad (1)$$

where $j = (-1)^{0.5}$, ω is angular frequency, $\rho(\mathbf{x})$ is density at $\mathbf{x}$, $\hat{G}(\mathbf{x}_A,\mathbf{x},\omega)$ is pressure at $\mathbf{x}_A$ arising from a monopole source at $\mathbf{x}$, and $\partial_i\hat{G}(\mathbf{x}_A,\mathbf{x},\omega)$ is pressure at $\mathbf{x}_A$ from a dipole source at $\mathbf{x}$. Here, the asterisk (*) denotes complex conjugation (corresponding to time-reversal in the time domain) and n_i is the outward normal to integration boundary ∂D_1, where this boundary encloses the locations $\mathbf{x}_A$ and $\mathbf{x}_B$ [in this case, ∂D_1 need not span the free surface because the integrand is zero there].

By a simple process of crosscorrelation and integration, equation 1 determines the Green's function between two receivers. Similar expressions exist for differing source and receiver types and for elastic media (van Manen et al., 2005, 2006; Wapenaar and Fokkema, 2006).

Equation 1 requires both monopole and dipole sources; hence, it is difficult to apply in practice. To simplify this expression, Wapenaar and Fokkema (2006) assume that the region outside ∂D_1 is homogeneous (with propagation velocity c and mass density ρ) and that the boundary is a sphere with large radius. These assumptions lead to the expression

$$\hat{G}^*(\mathbf{x}_B,\mathbf{x}_A,\omega) + \hat{G}(\mathbf{x}_B,\mathbf{x}_A,\omega) = \frac{2}{\rho c}\oint_{\partial D_1} \hat{G}^*(\mathbf{x}_A,\mathbf{x},\omega)\hat{G}(\mathbf{x}_B,\mathbf{x},\omega)d^2\mathbf{x}, \quad (2)$$

where only monopole sources are required. True amplitudes may not be estimated correctly where these assumptions are not met, but the phase can still be recovered correctly (Korneev and Bakulin, 2006; Wapenaar and Fokkema, 2006). This expression requires sources that surround the medium of interest, which is impractical, so we now further approximate equation 2.

Consider the two-layer model of Figure 1a, of which the integration boundary ∂D_1 encloses a part. We assume that the deepest sources provide a relatively small contribution to the interreceiver surface

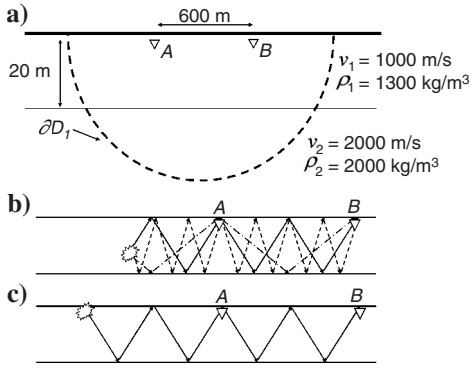

Figure 1. (a) Simple acoustic model used in initial testing. Receivers are labeled A and B, and surface ∂D_1 is shown (dashed). (b) An illustration of various multiple-raypaths from a source on the boundary ∂D_1 illustrated in (a). (c) Equivalent multiple-raypath to the solid ray in (b) but from a source at the surface. The source locations are stationary points for the multiples shown between the receiver pair A and B.

waves (contributing predominantly upgoing waves) and can be neglected. Furthermore, using simple geometric arguments and applying the stationary phase method of Snieder et al. (2006), we can show that for a stationary point on ∂D_1 (a position providing a dominant contribution to the interferometric integral), an equivalent stationary point exists at the surface (Figure 1b and c). This allows us to replace the integration over ∂D_1 in equation 2 by a summation over N surface source positions $\mathbf{x}_n$:

$$\hat{G}^*(\mathbf{x}_B,\mathbf{x}_A,\omega) + \hat{G}(\mathbf{x}_B,\mathbf{x}_A,\omega) = C\sum_{n=1}^{N} \hat{G}^*(\mathbf{x}_A,\mathbf{x}_n,\omega)\hat{G}(\mathbf{x}_B,\mathbf{x}_n,\omega), \quad (3)$$

where C is a scaling factor. Note that despite source points being at the free surface, this expression is nonzero because there are no derivatives present (c.f., equation 1).

Equation 3 is similar to equation 1 in Bakulin and Calvert (2004) but with a very different geometry using both surface sources and surface receivers. The results of Bakulin and Calvert (2004, 2006) show that despite the assumptions involved, expressions such as equation 3 can be effective when using real data, where the boundary of sources is neither spherical nor located within a homogeneous region.

Consider a group of multiples from a subsurface source that interfere to form a guided wave within the upper layer of Figure 1a. The acoustic guided wave is formed in a process similar to that of elastic surface waves (Shearer, 1999). From Figure 1b and c, we can see that stationary points exist at the surface for any order of reflection, similar to the findings of Sabra et al. (2005), contributing multiples (and hence guided waves) to equation 3. Therefore, an array of surface sources located in the region where we expect these guided-wave stationary points to occur could be used to stimulate the guided-wave component of the Green's function. Mehta et al. (2007) show that upgoing reflections provide a weak contribution when compared to the contribution of the direct wave (or guided wave, in this case). However, to ensure that any primary reflected-wave contribution to equation 3 is further minimized, we avoid placing sources near the locations where we expect primary reflection stationary points.

To demonstrate our method, we implement equation 3 in the simple 2D model shown in Figure 1a. Data are computed using a viscoelastic finite-difference code (Robertsson et al., 1994), with both attenuation and S-wave motion disabled. We first compute the Green's function between points A and B (located just below the free surface), band-limiting the result with a 25-Hz Ricker wavelet. This is illustrated as the dashed line throughout Figure 2. Three groups of waves can be seen. First, the refracted wave arrives from around 0.35 s. Then, higher-amplitude body waves (a combination of direct and reflected waves) arrive at around 0.6 s. The guided wave train arrives from around 0.8 s. This full Green's function is treated as representing our measured seismic survey data (obtained using a true source at either of the pair of receiver locations), from which we would wish to remove the guided-wave component.

Two sources located 40 m to the left of receiver A and to the right of receiver B (on the line where we expect guided-wave stationary points) are used to estimate the guided wave between the two receivers using equation 3, resulting in both an acausal estimate and a causal estimate (band-limiting as above, but after crosscorrelation). We consider only positive times in our analysis.

Figure 2a shows the estimated trace (solid line), with the full

Green's function plotted for reference (dashed line). The guided wave clearly dominates the estimate. After scaling the data to the guided-wave component, we plot the difference of these two signals in Figure 2b. The scale factor is related to (among other effects) the source amplitude and wavelet and the number of sources present. Note that, in the difference trace, most of the guided-wave energy has been removed, although the majority of the reflected wave remains.

If we have a full boundary of sources along ∂D_1 (i.e., applying equations 1 or 2 exactly), the guided-wave residual in Figure 2b is zero. The body waves are also annulled because when the boundary of sources encloses the medium of interest, the full and correct Green's function is obtained for both curves in Figure 2a. However, if we use a line of several sources at the surface, then at least some of these sources should lie at stationary points providing contributions to equation 3 that contain the correct interreceiver surface wave. When these crosscorrelations are stacked, the correct surface wave will sum constructively, and unwanted artifacts will interfere destructively. Then we may apply a spatial taper so that artifacts from the last few sources on the line do not remain uncancelled. Also, in heterogeneous media, secondary sources generated by lateral and vertical scattering of waves may supplement the source distribution, improving the results of equation 3 (Larose et al., 2005).

Therefore, we repeat the above experiment using eight sources (with offsets of 20, 40, 60, and 80 m on either side of the receiver pair), summing and subtracting the estimated guided waves (Figure 2c and d). As expected, the fit of the guided wave is improved in this case, resulting in a smaller residual in the difference trace. In both examples, artifacts have affected the earlier part of the data. If necessary, the subtraction can be made in a certain *t-x* or *f-k* window, preserving these early arrivals and allowing the advantages of the *f-k* method to be combined with our new method.

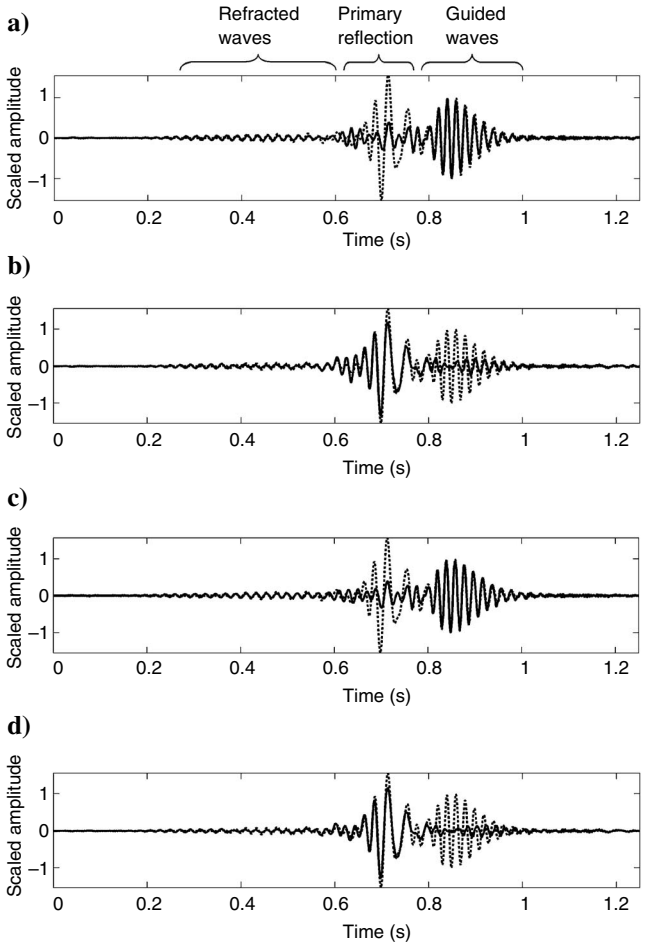

Figure 2. (a) The directly computed Green's function (dashed line), with the interferometrically estimated guided wave from one source pair superimposed (solid line). (b) The difference after scaling between the time series in (a), superimposed on the directly modeled Green's function. Views (c) and (d) are similar to (a) and (b) except that four source pairs are used in the guided-wave estimate. Refracted waves, primary reflection, and guided waves are labeled appropriately in (a).

ANELASTIC EXAMPLE

The model in Figure 1a was sufficiently simple to analyze quantitatively and intuitively the effect of varying the position and number of sources. However, to analyze the method's application to anelastic media using physical energy sources in the real earth, the test model should exhibit elastic surface waves (rather than acoustic guided waves), shear motion (hence mode conversions and Rayleigh waves), medium changes at depth producing deeper reflections (of interest in reflection seismology), and energy losses by attenuation.

Wapenaar and Fokkema (2006) show that it is possible to find an expression similar to equation 2 for elastic media requiring both P- and S-wave sources. These can be written as a sum of point forces. Assuming that the vertical component dominates when using vertical point forces (Herman and Perkins, 2006, test this assumption with field data), we implement equation 3 in the elastic case, using vertical particle velocity arising from a vertical force source only. Because of this approximation, we use a more sophisticated method of ground-roll subtraction (see below).

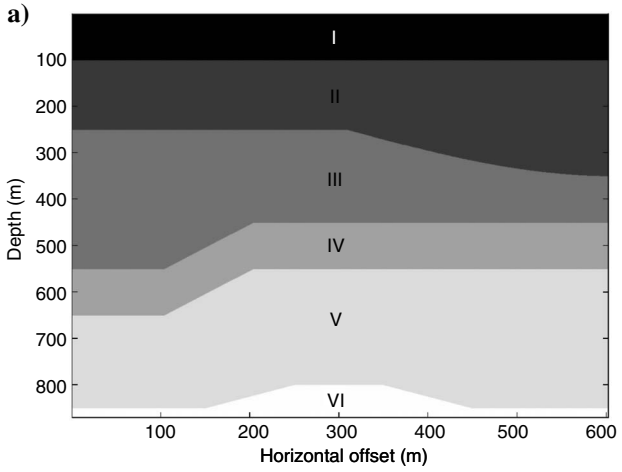

b)

Layer no.	v_p (m/s)	v_s (m/s)	ρ (kg/m^3)	Q_P	Q_S
I	1500	400	1700	150	100
II	1700	450	1800	10,000	10,000
III	2400	500	2000	10,000	10,000
IV	2750	600	2100	10,000	10,000
V	3000	700	2200	10,000	10,000
VI	4000	800	2500	10,000	10,000

Figure 3. (a) Model used for further testing. (b) Layer parameters.

We introduce a more realistic 2D-layered anelastic model (Figure 3) with near-surface attenuation and property contrasts at depth producing more complex body-wave arrivals. Note that this also allows us to test the (elastic) interferometry theory in an earth-like, anelastic setting; our tests show that it is applicable in practice despite this relaxation of the underlying assumptions (Curtis et al., 2006).

Receivers are located on the free surface at horizontal locations from 50 to 550 m with a separation of 5 m, and a full common-source gather is generated by implementing a source at 50 m. A delta function is used as the source signature, and data are band-limited by convolving with a 30-Hz Ricker wavelet. Figure 4a illustrates the common-source gather, simulating recorded data from which ground roll is to be removed. This is scaled such that the reflections can be seen, although the lack of trace clipping emphasizes the fairly typical relative strength of the ground roll in this example.

Using reasoning similar to the acoustic case above, we implement sources on either side of the receiver array at horizontal locations from 5 to 40 m and from 560 to 595 m with a separation of 5 m (results do not depend critically on this chosen separation). We use traces recorded from these sources in an elastic equivalent of equation 3 to estimate the ground roll between all source and receiver pairs shown in Figure 4a (band-limiting after crosscorrelation). We apply tapers to the source arrays, as discussed in the last section, and depict the estimated ground roll in Figure 4b. To increase the fold, we add the acausal part of the constructed Green's function to the causal part because these should be approximately equal in this case.

Because of further interferometric approximations in this case (i.e., lossy media, lack of horizontal source components), a least-squares filtering approach is used to optimize subtraction of the estimated ground roll from the common-source gather (Claerbout, 1976; Dong et al., 2006). For real data, equation 3 must be modified to include source signatures that are squared during crosscorrelation, but filtering can also account for this change in source signature.

In this example, we concatenate five neighboring channels of recorded data into a single trace: $d_c(t) = [d_1(t)\ d_2(t)\ d_3(t)\ d_4(t)\ d_5(t)]$. The five equivalent channels of interferometric data are also concatenated into a single trace, $g_c(t) = [g_1(t)\ g_2(t)\ g_3(t)\ g_4(t)\ g_5(t)]$, where $d_n(t)$ and $g_n(t)$ are the nth selected traces of recorded and interferometric data, respectively. The window of five channels is centered, in turn, on each receiver of interest, and the difference between the two is minimized using a standard least-squares filtering procedure. The concatenated traces have 11,824 samples, and we choose a

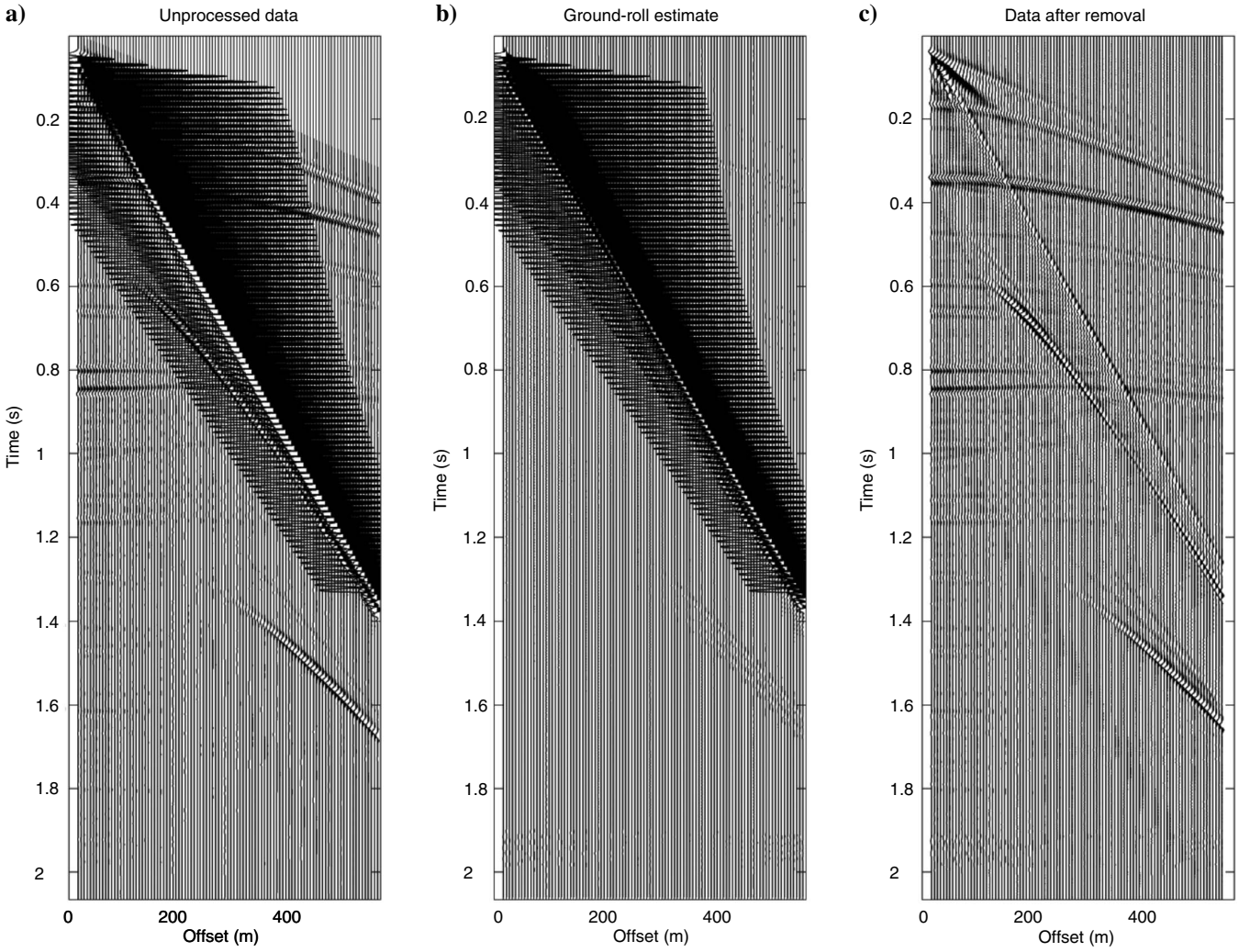

Figure 4. (a) Common-source gather from the model in Figure 3. (b) Interferometrically estimated ground roll. (c) Records in (a) after filtering and subtraction of records in (b). The offset is measured from the source location to each receiver.

filter of length 300. After filtering, only the central trace is used. Thus we filter the central trace using a filter designed from that and four neighboring traces.

The filtered interferometric data are subtracted from the common-offset gather. Figure 4c shows the resulting data. The ground roll has been suppressed effectively, while body waves crossing the ground roll have been mostly preserved during the filtering process, as desired.

CONCLUSIONS

We have illustrated synthetically that acoustic and anelastic surface waves propagating between two surface locations can be predicted and removed using seismic interferometry. We isolate the surface waves by locating surface sources on the line where we expect surface-wave stationary points to occur, and artifacts can be reduced by using an array of several such sources.

With a simple acoustic case, we explained intuitively in terms of stationary points why surface waves can be estimated using surface sources. A more realistic, anelastic model illustrated the promise of the method in land seismics; most of the surface wave in the synthetic survey data is removed using our method, although deeper body-wave reflections are preserved.

The examples presented are in two dimensions. Although the geometric spreading factors change in 3D media, relative amplitudes of (reflected) body waves and surface waves do not change significantly from the 2D case. Therefore, we would expect similar results for direct surface waves in 3D media. When scattered surface waves are present, surface sources also may be required at offline locations because we expect crossline scattered surface-wave stationary points.

In practice, the sources used for interferometry could constitute other sources used to create shot gathers in the survey and point-receiver data would be used (prior to group forming). Consequently, requirements of interferometric surface-wave removal may have to be considered during design of the survey for sufficient sources and receivers at appropriate locations to be included, as discussed above.

We expect that this method might be particularly advantageous in the presence of crossline scattered ground roll. Suppression of such ground roll is problematic using conventional methods such as f-k filtering: ground roll is often spread over a large range of wave vectors, making filter design difficult. However, because interferometry is applicable in any degree of heterogeneity and has been shown to improve in the presence of scatterers, the method may be able to isolate and suppress both the direct and scattered ground roll. We will test this on real data and report as results become available.

REFERENCES

Bakulin, A., and R. Calvert, 2004, Virtual source: New method for imaging and 4D below complex overburden: 74th Annual International Meeting, SEG, Expanded Abstracts, 2477–2480.

——, 2006, The virtual source method: Theory and case study: Geophysics, **71**, no. 4, SI139–SI150.

Claerbout, J., 1976, Fundamentals of geophysical data processing: Blackwell Scientific Publications, Inc.

Curtis, A., P. Gerstoft, H. Sato, R. Snieder, and K. Wapenaar, 2006, Seismic interferometry — Turning noise into signal: The Leading Edge, **25**, 1082–1092.

Dong, S., R. He, and G. Schuster, 2006, Interferometric prediction and least-squares subtraction of surface waves: 76th Annual International Meeting, SEG, Expanded Abstracts, 2783–2786.

Herman, G. C., and C. Perkins, 2006, Predictive removal of scattered noise: Geophysics, **71**, no. 2, V41–V49.

Korneev, V., and A. Bakulin, 2006, On the fundamentals of the virtual source method: Geophysics, **71**, no. 3, A13–A17.

Larose, E., A. Derode, D. Clorennec, L. Margerin, and M. Campillo, 2005, Passive retrieval of Rayleigh waves in disordered elastic media: Physical Review E, **72**, 046607.

Mehta, K., A. Bakulin, J. Sheiman, R. Calvert, and R. Snieder, 2007, Improving the virtual source method by wavefield separation: Geophysics, **72**, no. 4, V79–V86.

Robertsson, J. O. A., J. Blanch, and W. Symes, 1994, Viscoelastic finite-difference modeling: Geophysics, **59**, 1444–1456.

Sabra, K. G., P. Roux, and W. A. Kuperman, 2005, Arrival-time structure of the time-averaged ambient noise cross-correlation function in an oceanic waveguide: Journal of the Acoustical Society of America, **117**, 164–174.

Shapiro, N., and M. Campillo, 2004, Emergence of broadband Rayleigh waves from correlations of the ambient seismic noise: Geophysical Research Letters, **31**, L07614; http://dx.doi.org/10.1029/2004GL019491.

Shapiro, N., M. Campillo, L. Stehly, and M. Ritzwoller, 2005, High-resolution surface-wave tomography from ambient seismic noise: Science, **307**, 1615–1617.

Shearer, P., 1999, Introduction to seismology: Cambridge University Press.

Snieder, R., K. Wapenaar, and K. Larner 2006, Spurious multiples in seismic interferometry of primaries: Geophysics, **71**, no. 4, SI111–SI124.

van Manen, D. J., A. Curtis, and J. O. A. Robertsson, 2006, Interferometric modeling of wave propagation in inhomogeneous elastic media using time reversal and reciprocity: Geophysics, **71**, no. 4, SI47–SI60.

van Manen, D. J., J. O. A. Robertsson, and A. Curtis, 2005, Modeling of wave propagation in inhomogeneous media: Physical Review Letters, **94**, 164301.

Wapenaar, K., 2004, Retrieving the elastodynamic Green's function of an arbitrary inhomogeneous medium by cross correlation: Physical Review Letters, **93**, 254301.

Wapenaar, K., and J. Fokkema, 2006, Green's function representations for seismic interferometry: Geophysics, **71**, no. 4, SI33–SI46.